

Stacking-Engineered Thermal Transport and Phonon Filtering in Rhenium Disulfide

Yongjian Zhou¹‡, Haoran Cui²‡, Zefang Ye¹‡, Jung-Fu Lin³, Yan Wang² and Yaguo Wang¹**

1. Walker Department of Mechanical Engineering, The University of Texas at Austin, Austin, TX, 78712, USA
2. Department of Mechanical Engineering, University of Nevada, Reno, Reno, NV 89557, USA
3. Department of Geological Sciences, Jackson School of Geosciences, The University of Texas at Austin, 2305 Speedway Stop C1160, Austin, Texas 78712, USA

E-mails: yaguo.wang@austin.utexas.edu, yanwang@unr.edu.

‡These authors contributed equally.

KEYWORDS: Phonon filtering, stacking-order engineering, thermal transport, Van der Waals materials

ABSTRACT: Cross-plane heat transport is a critical bottleneck for van der Waals (vdW) electronics, yet its microscopic governing principles remain elusive. We demonstrate that stacking order is an effective control knob for cross-plane phonon transport in multilayer

Rhenium Disulfide (ReS₂). Thickness-dependent thermal conductivity measurements reveal remarkably long cross-plane phonon mean free paths (MFPs) ($\gtrsim 200$ –300 nm) and provide a direct experimental observation of the transition from quasi-ballistic transport to a thickness-independent ballistic limit. AA stacking exhibits nearly double the cross-plane thermal conductivity of AB stacking, driven by longer acoustic phonon lifetimes from a more “coherent” interlayer registry. Integrated deep neural-network molecular dynamics reveals that phonon filtering in ReS₂ is fundamentally frequency-selective: weak vdW coupling acts as a low-pass filter, whereas stronger coupling broadens the transmission passband. These results establish ReS₂ as a model system where stacking order and interlayer coupling can be engineered to tune heat conduction across diffusive, quasi-ballistic, and ballistic regimes, offering a new framework for thermal management in 2D electronics.

ReS₂ has emerged as a versatile two-dimensional (2D) material that is widely investigated for photodetectors, ultrafast saturable absorbers, and other optoelectronic applications owing to its high photoresponsivity, broadband absorption, and strong nonlinear optical response.^[1-3] ReS₂ crystallizes in a distorted 1T triclinic structure in which rhenium atoms form zigzag chains. This low-symmetry lattice dramatically enhances in-plane anisotropy and, when combined with weak interlayer vdW coupling, endows ReS₂ with physical properties that are highly sensitive to structural registry. Multilayer ReS₂ can adopt two well-defined stacking orders: a “coherent” AA registry with perfectly aligned layers, and an AB configuration defined by a half-unit-cell lateral shift, which correspond to distinct local energy minima within the crystal lattice.^[4] These stacking configurations exert strong influence on the material’s vibrational, optical, and electronic responses. As such, stacking order constitutes an additional and independent structural

degree of freedom for tuning the properties of ReS_2 , beyond layer number and in-plane orientation. [5-7]

Similar to other vdW materials, ReS_2 exhibits strongly anisotropic thermal transport, with in-plane thermal conductivity ($\sim 70 \text{ W m}^{-1} \text{ K}^{-1}$ along Re-chain and $\sim 50 \text{ W m}^{-1} \text{ K}^{-1}$ perpendicular to Re-chain) substantially exceeding its cross-plane counterpart ($\sim 0.55 \text{ W m}^{-1} \text{ K}^{-1}$ in nanofilms), as reported by prior time-domain thermoreflectance (TDTR) measurements.^[8] In vdW-based electronic and optoelectronic devices, heat generated in the active layers dissipates predominantly along the cross-plane direction through stacked layers and interfaces, making cross-plane thermal conductivity (κ_c) a critical bottleneck for device performance and reliability.^[9] Understanding how interlayer registry controls cross-plane phonon transport is therefore essential for engineering next-generation vdW electronics and optoelectronics. Historically, cross-plane thermal transport in layered vdW materials was assumed to be dominated by phonons with very short MFPs, typically on the order of only a few nanometers. This picture has been fundamentally revised by recent experimental and theoretical studies on benchmark systems such as graphite^[10-12] and MoS_2 ^[13], which demonstrate that room-temperature cross-plane phonon MFPs can extend to hundreds of nanometers. Such unexpectedly long-range transport has been attributed to a phonon filtering effect, in which weak interlayer vdW interactions suppress short-MFP phonons and confine heat flow to long-MFP modes.

ReS_2 presents a unique and largely unexplored opportunity to examine cross-plane phonon transport in exceptional depth. Because its AA and AB stacking sequences remain remarkably stable across varying thicknesses, ReS_2 serves as an ideal platform for investigating and ultimately engineering cross-plane heat transport in ultrathin vdW devices. While earlier TDTR

measurements reported no clear thickness dependence for ReS_2 films between 60 nm and 450 nm, these studies did not distinguish between stacking orders and therefore effectively averaged over fundamentally different interlayer configurations.^[8] Consequently, the role of interlayer registry in governing phonon filtering, phonon MFPs, and the crossover between distinct transport regimes remains a critical and practically important open question.

In this work, we perform systematic picosecond transient thermoreflectance (ps-TTR) measurements of high-quality ReS_2 samples with well-defined AA or AB stacking orders that persists over micrometer-scale thicknesses. These measurements are thus capable of capturing an order-or-magnitude variation in κ_c with increasing sample thickness, as well as pronounced differences between AA- and AB-stacked ReS_2 . By integrating the ps-TTR measurements with molecular dynamics simulations based on a deep neural network (DNN) potential trained from ab initio, we further compare the spectral phonon properties of AA- and AB-stacked ReS_2 for both ambient pressure and high-pressure conditions. Through this combined experimental-computational approach, we elucidate the unique phonon transport behavior of ReS_2 and demonstrate it as a model system in which stacking order, interlayer coupling, and phonon filtering can be deliberately manipulated to tune cross-plane heat conduction from diffusive to quasi-ballistic and fully ballistic regimes.

Figs. 1a and 1b show the atomic configurations of the AA and AB stacking orders in ReS_2 . The stacking order of ReS_2 samples can be easily identified by measuring the difference between two Raman peaks: $\Delta = \text{mode III} - \text{mode I}$. For AA stacking, $\Delta \sim 13 \text{ cm}^{-1}$, and for AB stacking, $\Delta \sim 20 \text{ cm}^{-1}$. We employed a re-exfoliation approach to confirm that a single, well-defined stacking order can persist over thicknesses of several micrometers. (Fig. S1 & S2) Cross-plane thermal conductivities were measured using a ps-TTR technique ^[14, 15]. The thickness-dependent κ_c for both AA- and AB-stackings are presented in Fig. 1c. In the ultrathin regime (below 100 nm), both stacking configurations exhibit similar values, which is consistent with prior measurements ^[8] and suggests that thermal transport in the thinnest flakes is primarily constrained by boundary scattering. However, as thickness increases, the thermal behaviors of the two registries diverge significantly. While both configurations show a pronounced increase in κ_c with thickness, AA-stacked samples exhibit a more rapid rise and reach a clear saturation plateau of approximately $4.0 \text{ W m}^{-1} \text{ K}^{-1}$. In contrast, AB stacking exhibits a slower recovery of κ_c and fails to reach saturation even as thicknesses approach 1 μm , trending toward an extrapolated bulk limit of approximately $2.0 \text{ W m}^{-1} \text{ K}^{-1}$. This distinct bifurcation demonstrates that stacking order serves as a primary determinant of intrinsic cross-plane transport, while the delayed saturation in both registries provides direct experimental evidence of exceptionally long cross-plane phonon MFPs that far exceed the predictions of conventional kinetic theory.

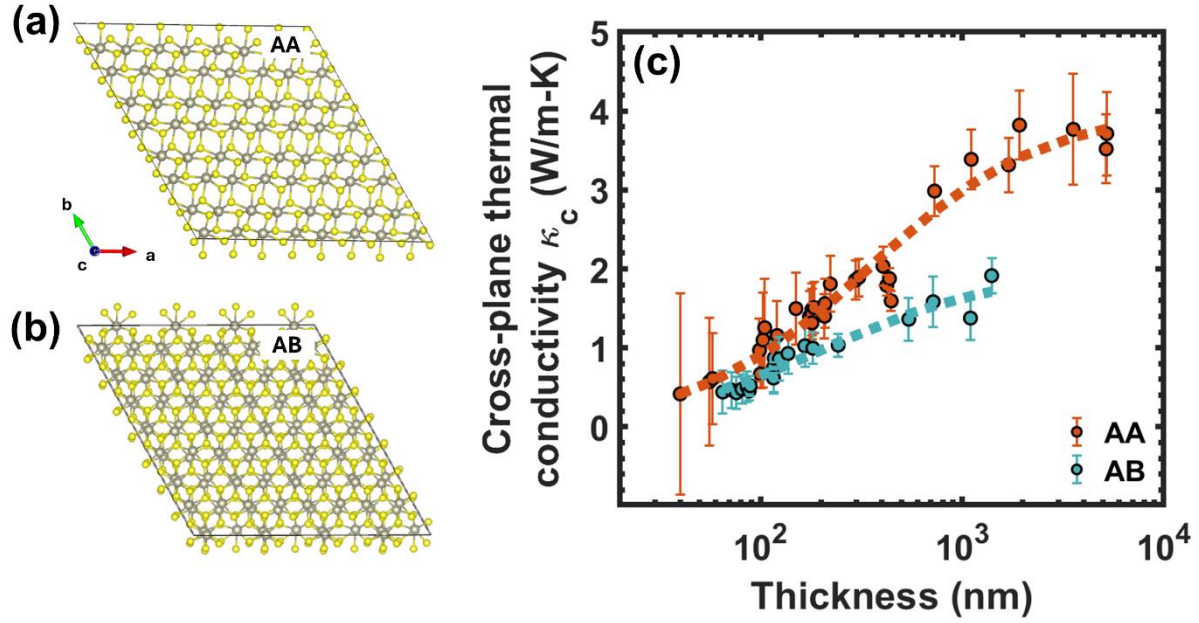


Figure 1. (a,b) Atomic structures of AA and AB stacking orders, where grey dots represent Re atoms and yellow dots represent S atoms. (c) Measured cross-plane thermal conductivity as a function of thickness for AA- and AB-stacked ReS_2 . Dashed lines represent fittings with gray model.

To quantify the characteristic MFPs, we fit the experimental κ_c using the gray model^[16, 17],

$$\kappa_{film} = \kappa_{bulk} \frac{d}{d + \Lambda_{bulk}}$$

The extracted bulk κ_c values agree with the experimental saturation trends: $\sim 4.0 \text{ W m}^{-1} \text{ K}^{-1}$ for AA stacking and $\sim 2.0 \text{ W m}^{-1} \text{ K}^{-1}$ for AB stacking. The corresponding bulk phonon MFPs are remarkably long, $\sim 346 \text{ nm}$ for AA and $\sim 203 \text{ nm}$ for AB. If we apply the kinetic expression: $\kappa_c \sim 1/3 C \nu_c \Lambda_c$, where C is heat capacity and ν_c is cross-plane sound velocity, yields $\Lambda_c \approx 2.2 \text{ nm}$ for AA stacking, corresponding to only ~ 8 layers. The experimental MFPs surpass kinetic theory predictions by nearly two orders of magnitude. This striking discrepancy arises because conventional kinetic theory fails to distinguish between the short-MFP modes that dominate heat capacity and the long-wavelength phonons that drive thermal transport. By using the total heat

capacity, the kinetic model systematically underestimates the effective MFPs of the primary heat-carrying phonons. Resolving these mode-dependent characteristics requires a detailed spectral analysis.

Fig. 1 highlights two critical findings: first, κ_c is highly sensitive to stacking order, with AA stacking conducting heat nearly twice as efficiently as the AB configuration. Second, both registries exhibit exceptionally long phonon MFPs, confirming that cross-plane transport in ReS_2 is dominated by long-range modes rather than localized vibrations. These observations raise fundamental questions regarding why AA stacking supports much higher conductivity and what physical mechanism drives such long MFPs, which we address through mode-resolved spectral analysis in the following sections.

To address the first question: why AA-stacking ReS_2 conducts heat more efficiently than its AB-stacking, we constructed a DNN interatomic potential, using the DeepMD approach ^[18], from extensive ab initio data for both stacking orders and performed mode-resolved phonon analysis. The accuracy of the DNN potential was validated through non-equilibrium molecular dynamics (NEMD) simulations ^[19] performed at 300 K using LAMMPS ^[20]. As demonstrated in Fig. S4, the NEMD results reproduce the experimentally measured κ_c for both stacking orders up to ~ 300 nm, confirming that the DNN potential reliably captures the size-dependent thermal transport in both types of ReS_2 .

Bulk-limit thermal conductivities were subsequently obtained using equilibrium molecular dynamics (EMD) [21] and the Green–Kubo formalism [22, 23]. The predicted bulk κ_c values are approximately $4.5 \text{ W} \pm 0.12 \text{ m}^{-1} \text{ K}^{-1}$ for AA stacking and $3.2 \pm 0.11 \text{ W m}^{-1} \text{ K}^{-1}$ for AB stacking, slightly higher than the experimental values, which is expected because defects and imperfections are present in experimental samples but are absent in simulations. Importantly, both experiments and simulations clearly show that AA-stacking structures possess significantly higher κ_c than their AB counterparts, underscoring the crucial role of stacking order in determining thermal transport in ReS_2 .

To identify the microscopic origin of this stacking-dependent behavior, we performed spectral energy density (SED) analysis [24], which yields phonon dispersions, mode-resolved phonon group velocities, lifetimes and MFPs. Fig. 2a displays the phonon dispersion relations obtained from the SED calculations. The LA branch in AA-stacking ReS_2 exhibits a slightly steeper slope compared to AB-stacking ReS_2 , while the two TA branches are nearly degenerate in AA stacking but clearly split in the AB case, consistent with our density functional theory (DFT) calculations (Fig. S7). The corresponding group velocities (Fig. 2b) show that LA velocities in AA are higher than in AB, whereas AB exhibits higher TA velocities. However, the difference in group velocities is not sufficiently large to account for AA's substantially higher κ_c .

Figs. 2c and 2d show that both LA and TA phonons in AA-stacking ReS_2 possess systematically and notably longer lifetimes than those in AB-stacking configuration, which is the primary origin of the higher κ_c in AA stacking. The longer phonon lifetimes of AA-stacking ReS_2 originates from the near-degeneracy of its TA modes, which limits the available three-phonon scattering channels due to more stringent energy-conservation conditions. In contrast, the TA-mode splitting in AB-stacking ReS_2 opens additional allowed scattering pathways, thereby increasing anharmonic phonon scattering and reducing lifetimes. Due to its relatively longer phonon lifetimes, AA-stacking ReS_2 has notably higher contribution to κ_c by longer-MFP modes than its AB-stacking counterpart, as revealed by the mode-wise κ_c and cumulative κ_c data in Fig. 2e. Fig. 2f further illustrates this behavior by comparing the three-phonon emission phase space, where one higher-frequency TA mode splits into two lower-frequency modes. The AB-stacking structure exhibits a markedly larger scattering phase space than its AA-stacking counterpart. This interpretation is consistent with the structural configurations in Fig. 1: AA stacking features perfect vertical alignment between adjacent layers, a more “coherent” interlayer registry, while AB stacking introduces a half-unit-cell lateral shift. This structural mismatch in AB stacking naturally increases phonon scattering across layers and lowers the κ_c .

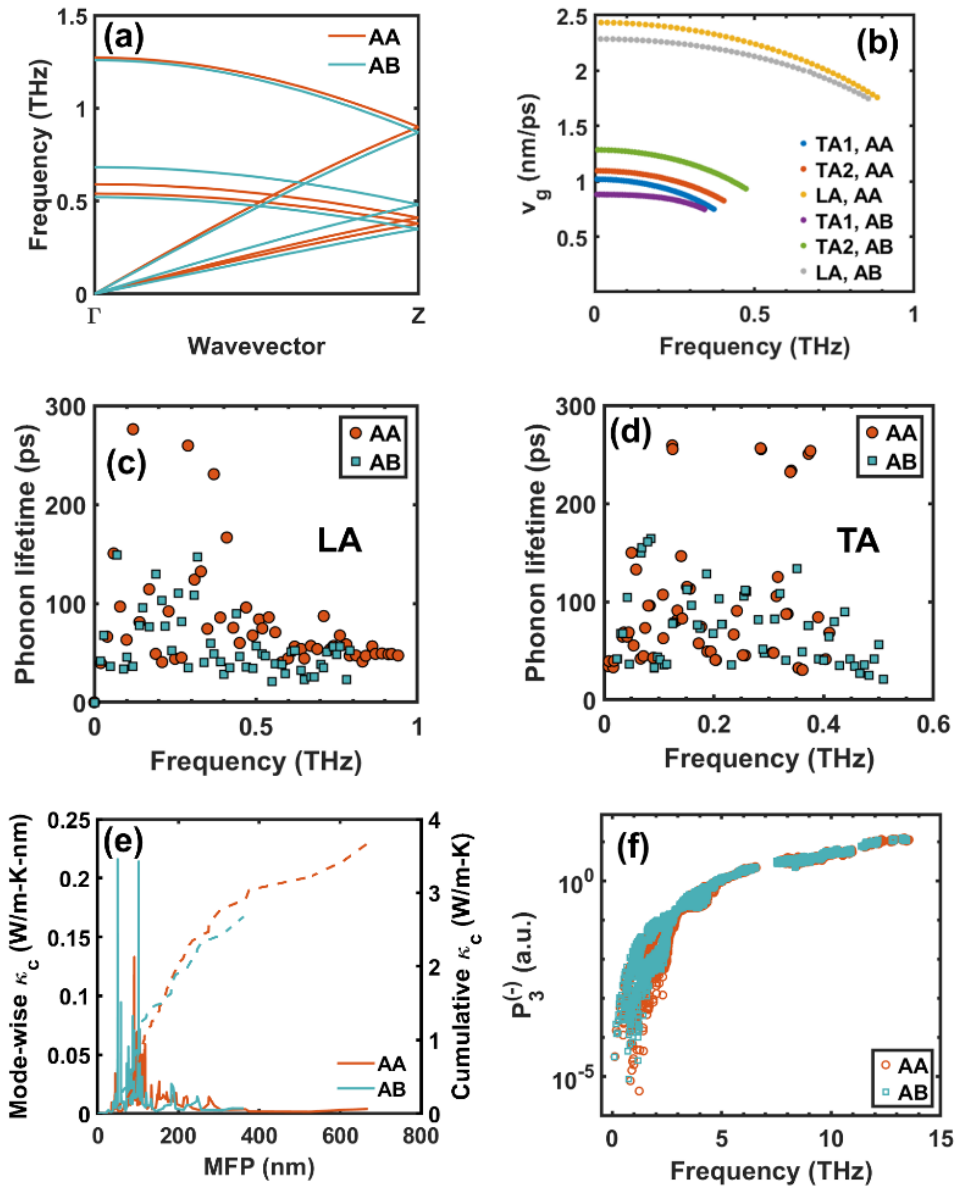


Figure 2. Mode-resolved phonon properties of AA- and AB-stacked ReS₂ from SED calculations. (a) Phonon dispersion relations for AA and AB stacking. (b) Mode-resolved phonon group velocities. (c,d) Phonon lifetimes for AA and AB stacking extracted from Lorentzian fitting of SED spectra. (e) Left axis: mode-wise cross-plane thermal conductivity. Right axis: cumulative cross-plane thermal conductivity. (f) The emission process of three-phonon scattering phase space for ReS₂ with AA and AB stacking orders.

We now address the second question: what governs the long phonon MFP. Similar thickness-dependent measurements on graphite and MoS₂ consistently indicate that long-MFP phonons dominate cross-plane heat conduction. In graphite, the c-axis phonon MFP has been estimated to be ~ 200 nm,^[10, 11] while in MoS₂, phonons with MFPs exceeding ~ 200 nm contribute more than 50% of the total κ_c ^[12]. These unexpectedly long MFPs have been attributed to the so-called phonon filtering effect, in which the weak interlayer vdW forces suppress short-MFP phonons and preferentially allow long-MFP modes to transmit across layers. If this conventional understanding of phonon filtering effect holds, one would expect the filtering effect to depend strongly on interlayer bonding strength: weaker vdW force \rightarrow stronger filtering \rightarrow a larger contribution from longer-MFP phonons (i.e., a spectral shift of mode-wise κ_c toward longer MFP), and conversely, stronger interlayer coupling should weaken filtering and contribution from short-MFP phonons should increase (i.e. a spectral shift of mode-wise κ_c toward shorter MFP).

Hydrostatic pressure is a convenient tool to tune interlayer force in vdW materials and test this conventional picture of phonon filtering effect. Hydrostatic pressure was applied using a Nosé-Hoover barostat [25, 26] in all three directions. We calculated the cumulative κ_c as a function of MFP for both AA and AB stackings at 0 GPa and 20 GPa. As shown in Figs. 3a and 3c, increasing pressure (i.e., strengthening interlayer coupling) shifts the cumulative κ_c curves toward longer MFPs for both stackings. For AA stacking, phonons with $\Lambda < 180$ nm contribute 50% of κ_c at 0 GPa, but the 50% cutoff increases to ~ 300 nm at 20 GPa. For AB stacking, the cutoff shifts from ~ 120 nm at 0 GPa to above 200 nm at 20 GPa. The corresponding mode-wise κ_c spectra (Fig. 3b and 3d) further confirm that stronger inter-layer force at higher pressure extends the phonon contribution into the long-MFP regime. This trend arises because applying pressure increases the group velocity $v_c(\omega)$, while phonon lifetimes $\tau(\omega)$ change only weakly (shown in Fig. S8); as a result, the MFP $\Lambda_c(\omega) = v_c(\omega)\tau(\omega)$ becomes longer even though the spectral filter becomes less selective. These observations seem to contradict the conventional understanding of phonon filtering and indicate that the relationship between phonon filtering and MFP requires careful re-examination.

Because phonon filtering is fundamentally a spectral (frequency-domain) phenomenon, we next analyzed cumulative κ as a function of phonon frequency (Fig. 4). At 0 GPa, both AA and AB stacking show that $\sim 50\%$ of the κ_c arises from phonons around 0.3 THz (Fig. 4a), and virtually all contributing modes lie below ~ 0.5 THz (Fig. 4b). When pressure increases to 20 GPa, however, the transmission bandwidth broadens dramatically, extending to ~ 1.5 THz (Fig. 4d and 4f), and the cumulative κ_c curves gain substantial weight at higher frequencies (Fig. 4c and 4e). This indicates that weak vdW forces at low pressure act as a strong low-pass *spectral* filter, effectively blocking high-frequency modes and transmitting only long-wavelength phonons.

We quantify the filtering strength using a cutoff frequency $\omega_{\text{cut}}=0.5$ THz, defined as $F(\omega_{\text{cut}}) = \kappa(\omega < \omega_{\text{cut}})/\kappa_{\text{max}}$. For AA stacking, F increases from 37.22% at 20 GPa to 78.4% at 0 GPa; for AB stacking, it increases from 35.97% to 80.0% over the same pressure range. These values demonstrate that the filtering strength is controlled predominantly by the vdW interlayer force, rather than the stacking order.

We define the phonon filtering effect as the preferential transmission of low-frequency, long-wavelength modes across the vdW gap, which suppresses high-frequency contributions to cross-plane heat flow. Because this mechanism originates from the wave nature of phonons^[27], it is most naturally described in the frequency domain and is closely analogous to optical low-pass filtering.^[28] This definition resolves the ambiguity in the literature^[29, 30], where the thermal consequences of filtering are often expressed in the MFP domain, since Λ determines how far each transmitted mode carries heat. Our results show that these two perspectives must be considered together: phonon filtering is fundamentally a spectral effect, and weaker interlayer coupling narrows the phonon bandwidth (stronger filtering at 0 GPa, Fig. 4), whereas the MFP spectrum reflects the transport outcome of the modes that pass through that filter, resulting in shorter Λ at 0 GPa due to lower phonon group velocities (Fig. 3).

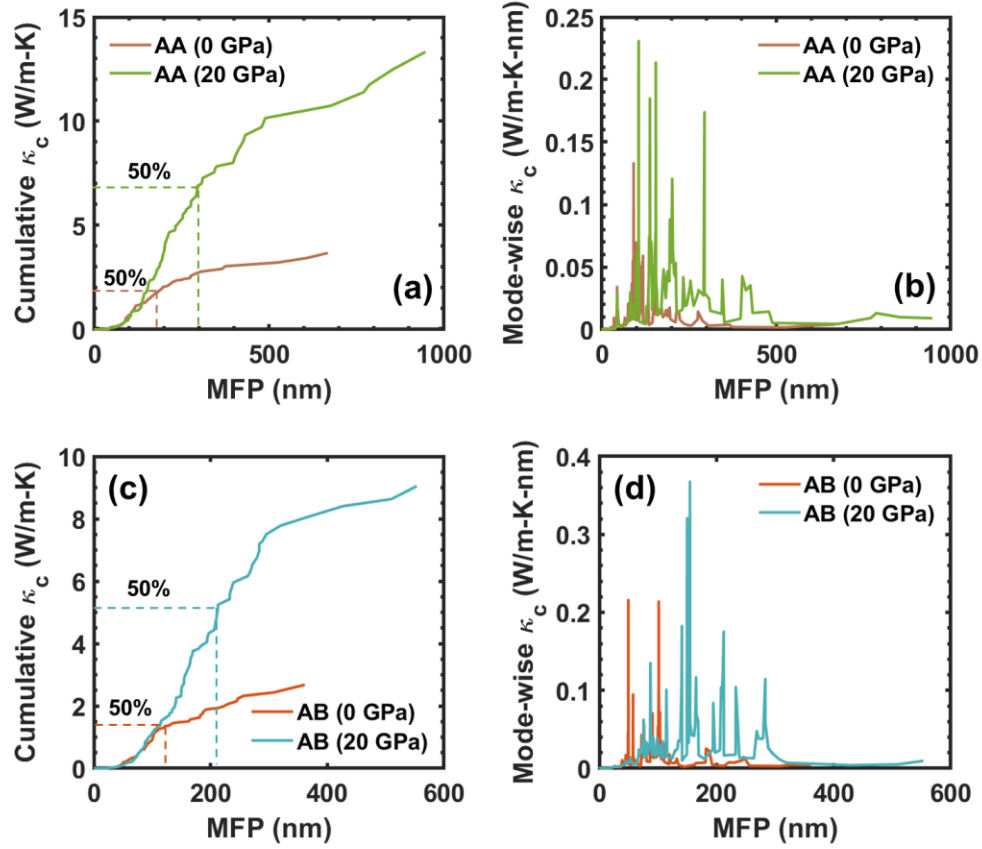


Figure 3. Cumulative cross-plane thermal conductivity as a function of phonon MFP for AA- and AB-stacked ReS_2 under different pressures. (a,c) Cumulative cross-plane thermal conductivity versus MFP at 0 GPa and 20 GPa for AA and AB stacking. (b,d) Corresponding mode-wise cross-plane thermal conductivity spectra displaying the distribution of phonon contributions across MFPs.

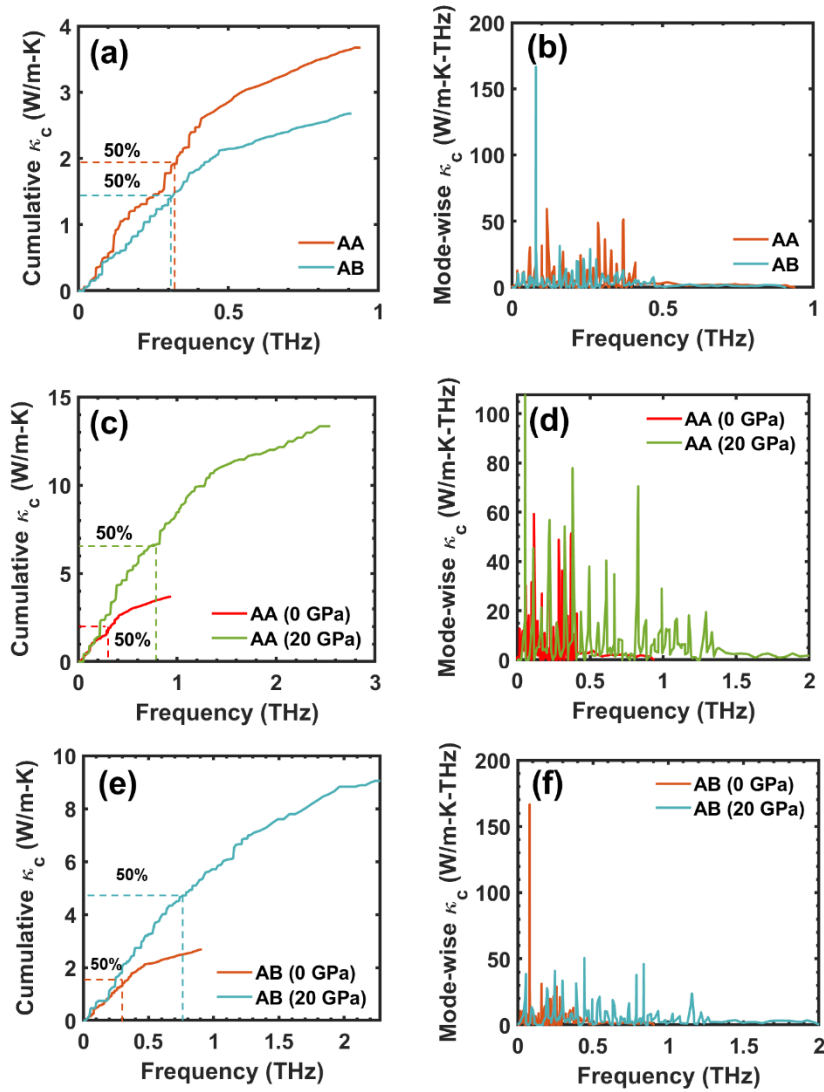


Figure 4. Cumulative cross-plane thermal conductivity as a function of phonon frequency for AA- and AB-stacked ReS₂ under different pressures. (a,c,e) Cumulative cross-plane thermal conductivity versus frequency at 0 GPa and 20 GPa for AA and AB stacking. (b,d,f) Corresponding mode-wise cross-plane thermal conductivity spectra displaying the distribution of phonon contributions in the frequency domain.

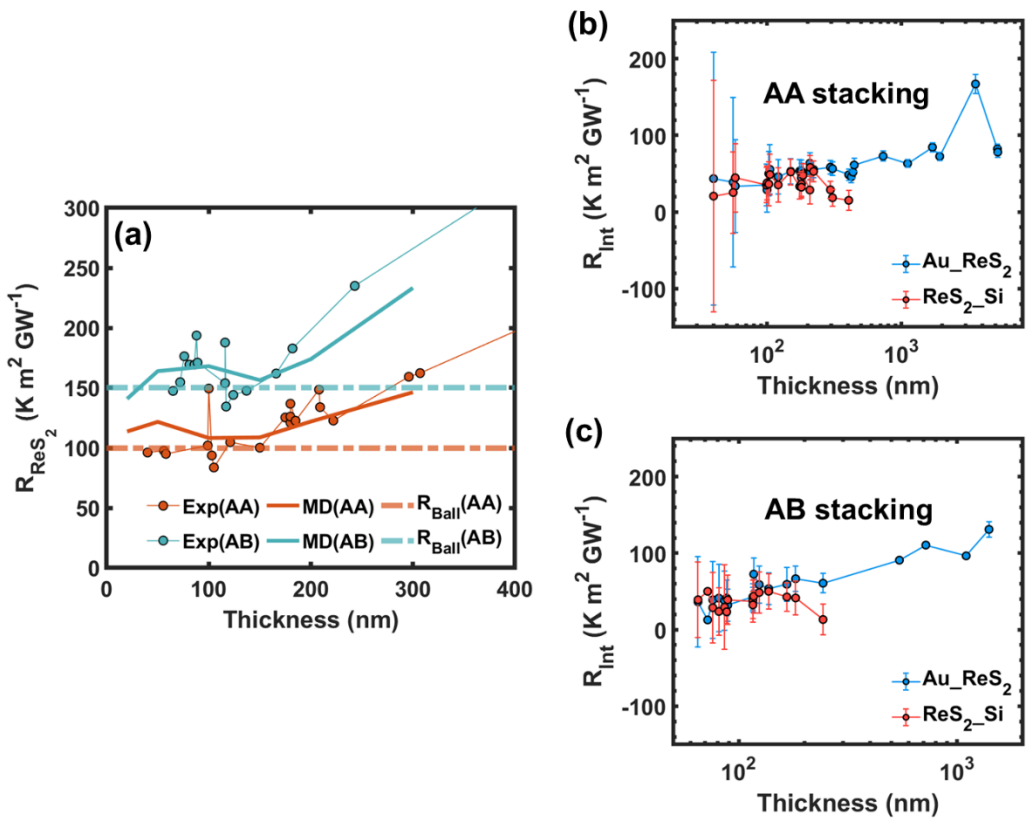


Figure 5. (a) Thickness-dependent cross-plane thermal resistance of AA- and AB-stacked ReS_2 , with corresponding NEMD simulation results. (b) Thickness-dependent contact resistances at the Au/ ReS_2 and ReS_2 /Si interfaces for AA-stacked samples. (c) Thickness-dependent contact resistances at the Au/ ReS_2 and ReS_2 /Si interfaces for AB-stacked samples.

To further elucidate the thickness dependence of cross-plane heat transport, the measured κ_c was converted to thermal resistance using $R=t/\kappa_c$, where t is the film thickness. As shown in Fig. 5a, the resistance of ReS_2 does not decrease linearly with thickness, but instead exhibits a sublinear, saturating trend as thickness decreases, a hallmark of quasi-ballistic transport [13, 31], in which phonon MFPs are comparable to the film thickness. In the thinnest flakes (<150 nm), both AA- and AB-stacked samples display a clear plateau in resistance, indicating that the heat flow has transitioned into the fully ballistic regime where the conductance becomes thickness-independent. [32, 33] This behavior is faithfully reproduced by our NEMD simulations. From the magnitude of the plateau, we extract ballistic thermal resistances of $R_{\text{ball}} \approx 150 \text{ m}^2 \text{ K GW}^{-1}$ for AB stacking and $\approx 100 \text{ m}^2 \text{ K GW}^{-1}$ for AA stacking, values an order of magnitude larger than those reported for MoS_2 ($\sim 10 \text{ m}^2 \text{ K GW}^{-1}$) [13]. Fig. 5b & 5c present the corresponding thickness-dependent contact resistances for both stacking orders. The contact resistances show no systematic dependence on thickness, and the values at the Au/ ReS_2 interface ($\sim 50 \text{ m}^2 \text{ K GW}^{-1}$, or $20 \text{ MW m}^{-1} \text{ K}^{-1}$) agree well with previously reported TDTR measurements and further confirms that the thickness dependent trends do come from intrinsic thermal transport in $R_{\text{ReS}2}$. [8]

The direct experimental observation of the ballistic limit in ReS_2 is a notable outcome of this study, enabled by two key factors. First, the ps-TTR technique, with its single-pulse excitation and long delay-time window, captures the intrinsic thermal response of ultrathin films without cumulative heating, allowing early-time ballistic transport to be resolved. Second, the exceptionally long and stacking-dependent cross-plane phonon MFPs in ReS_2 , arising from its weak and registry-sensitive vdW coupling, ensure that the condition $t \lesssim \Lambda_c$ is reached at experimentally accessible thicknesses, permitting the ballistic resistance plateau to emerge directly in the measurements. The resulting finite intercept R_{ball} represents the intrinsic ballistic resistance, reflecting the fundamental phonon transmission across atomic layers and setting the upper bound for heat dissipation in ultrathin ReS_2 . The substantially larger R_{ball} in ReS_2 compared with MoS_2 indicates a much lower intrinsic phonon transparency across its vdW gaps, consistent with a narrower spectral window that admits only low-frequency, long-wavelength phonons. The contrast between AA and AB stacking demonstrates that stacking order can serve as a practical tuning parameter for R_{ball} , enabling control over interlayer phonon transmission by modifying registry and coupling strength. Such tunability offers a new approach to engineering vdW thermal filters, phononic interfaces, and low-conductance barriers for 2D electronics and optoelectronic devices.

In summary, this work demonstrates that stacking order, an aspect largely neglected in prior studies of vdW materials, is a key determinant of cross-plane phonon thermal transport in ReS_2 , with implications for thermal transport engineering in ReS_2 and other vdW materials. By integrating systematic ps-TTR measurements on micron-scale crystals with single stacking order, and deep-learning-based molecular dynamics and SED analysis, we demonstrate that both AA and AB stacking orders support exceptionally long phonon MFP and exhibit distinct transitions

from quasi-ballistic to fully ballistic transport as sample thickness decreases below \sim 150 nm. Notably, AA-stacking ReS_2 exhibits significantly higher κ_c than its AB-stacking counterpart, which is attributed to longer acoustic phonon lifetimes enabled by a more "coherent" interlayer registry of AA stacking structure. Furthermore, pressure-dependent analyses reveal that phonon filtering in ReS_2 is a fundamentally frequency-selective mechanism, where weak vdW coupling enforces a low-pass filter that is highly tunable through interlayer coupling. These findings reconcile the distinct definitions of "coherence" held by the heat transfer and condensed matter physics communities by demonstrating that ReS_2 inherently exhibits both wave- and particle-like transport characteristics. We show that weak interlayer coupling at ambient pressure maintains phase correlation among long-wavelength phonons over hundreds of nanometers, whereas stronger coupling at high pressure increases the MFP primarily by enhancing phonon group velocities. By bridging the gap between the mean-free-path and coherence-length frameworks, serves as a unified platform for the spectral engineering of thermal transport across diverse vdW materials.

AUTHOR INFORMATION

Corresponding Authors

1. Yaguo Wang: Walker Department of Mechanical Engineering, The University of Texas at Austin, Austin, TX, 78712, USA; Email: yaguo.wang@austin.utexas.edu
2. Yan Wang: Department of Mechanical Engineering, University of Nevada, Reno, Reno, NV 89557, USA; Email: yanwang@unr.edu

Authors

1. Yongjian Zhou: Walker Department of Mechanical Engineering, The University of Texas at Austin, Austin, TX, 78712, USA.
2. Haoran Cui: Department of Mechanical Engineering, University of Nevada, Reno, Reno, NV 89557, USA.
3. Zefang Ye: Walker Department of Mechanical Engineering, The University of Texas at Austin, Austin, TX, 78712, USA.
4. Jun-Fu Lin: Department of Geological Sciences, Jackson School of Geosciences, The University of Texas at Austin, 2305 Speedway Stop C1160, Austin, Texas 78712, USA.

Acknowledgements

Yongjian Zhou, Zefang Ye and Yaguo Wang acknowledge the funding support from the National Science Foundation (NSF-CBET award no. 211660). Haoran Cui, and Yan Wang thank the support from the National Science Foundation (NSF-CBET award no. 2211696)

Notes

The authors declare no competing financial interest.

References

1. Shim, Jaewoo, Aely Oh, Dong-Ho Kang, Seyong Oh, Sung Kyu Jang, Jaeho Jeon, Min Hwan Jeon et al. "High-performance 2D rhenium disulfide (ReS₂) transistors and photodetectors by oxygen plasma treatment." *Advanced Materials* 28, no. 32 (2016): 6985-6992.
2. Su, Xiancui, Baitao Zhang, Yiran Wang, Guanbai He, Guoru Li, Na Lin, Kejian Yang, Jingliang He, and Shande Liu. "Broadband rhenium disulfide optical modulator for solid-state lasers." *Photonics Research* 6, no. 6 (2018): 498-505.
3. Meng, Xianghai, Yongjian Zhou, Ke Chen, Richard H. Roberts, Wenzhi Wu, Jung-Fu Lin, Ray T. Chen, Xiaochuan Xu, and Yaguo Wang. "Anisotropic saturable and excited-state absorption in bulk ReS₂." *Advanced Optical Materials* 6, no. 14 (2018): 1800137.
4. Zhou, Yongjian, Nikhilesh Maity, Amritesh Rai, Rinkle Juneja, Xianghai Meng, Anupam Roy, Yanyao Zhang et al. "Stacking-Order-Driven Optical Properties and Carrier Dynamics in ReS₂." *Advanced Materials* 32, no. 22 (2020): 1908311.
5. Zhou, Yongjian, Nikhilesh Maity, Jung-Fu Lin, Abhishek K. Singh, and Yaguo Wang. "Nonlinear optical absorption of ReS₂ driven by stacking order." *ACS Photonics* 8, no. 2 (2021): 405-411.
6. Zhou, Yongjian, and Yaguo Wang. "Wavelength and stacking order dependent exciton dynamics in bulk ReS₂." *Advanced Optical Materials* 10, no. 23 (2022): 2201322.
7. Chen, Yun, Jinguo Lin, Junjie Jiang, Danyang Wang, Yue Yu, Shouheng Li, Jun'an Pan et al. "Constructing slip stacking diversity in van der Waals homobilayers." *Advanced Materials* 36, no. 36 (2024): 2404734.
8. Jang, Hyejin, Christopher R. Ryder, Joshua D. Wood, Mark C. Hersam, and David G. Cahill. "3D anisotropic thermal conductivity of exfoliated rhenium disulfide." *Advanced Materials* 29, no. 35 (2017): 1700650.
9. Zhang, Lenan, Yang Zhong, Xin Qian, Qichen Song, Jiawei Zhou, Long Li, Liang Guo, Gang Chen, and Evelyn N. Wang. "Toward optimal heat transfer of 2D–3D heterostructures via van der Waals binding effects." *ACS Applied Materials & Interfaces* 13, no. 38 (2021): 46055-46064.
10. Zhang, Hang, Xiangwen Chen, Young-Dahl Jho, and Austin J. Minnich. "Temperature-dependent mean free path spectra of thermal phonons along the c-axis of graphite." *Nano letters* 16, no. 3 (2016): 1643-1649
11. Wei, Zhiyong, Juekuan Yang, Weiyu Chen, Kedong Bi, Deyu Li, and Yunfei Chen. "Phonon mean free path of graphite along the c-axis." *Applied Physics Letters* 104, no. 8 (2014).
12. John Crosby, Haoran Cui, Yan Wang; Significant ballistic thermal transport across graphene layers: Effect of nanoholes and lithium intercalation. *Appl. Phys. Lett.* 23 August 2025; 127 (8): 082201.
13. Sood, Aditya, Feng Xiong, Shunda Chen, Ramez Cheaito, Feifei Lian, Mehdi Asheghi, Yi Cui, Davide Donadio, Kenneth E. Goodson, and Eric Pop. "Quasi-ballistic thermal transport across MoS₂ thin films." *Nano letters* 19, no. 4 (2019): 2434-2442.

14. Jeong, Jihoon, Xianghai Meng, Ann Kathryn Rockwell, Seth R. Bank, Wen-Pin Hsieh, Jung-Fu Lin, and Yaguo Wang. "Picosecond transient thermoreflectance for thermal conductivity characterization." *Nanoscale and Microscale Thermophysical Engineering* 23, no. 3 (2019): 211-221.

15. Ye, Zefang, Janghan Park, Yanyao Zhang, Xianghai Meng, Matthew Disiena, Sanjay K. Banerjee, Jung-Fu Lin, and Yaguo Wang. "Simultaneous Determination of Thermal Conductivity and Heat Capacity in Thin Films with Picosecond Transient Thermoreflectance and Picosecond Laser Flash." *Nanoscale and Microscale Thermophysical Engineering* 27, no. 3-4 (2023): 182-194.

16. Majumdar, A. S. M. E. "Microscale heat conduction in dielectric thin films." (1993): 7-16.

17. Kaiser, Jan, Tianli Feng, Jesse Maassen, Xufeng Wang, Xiulin Ruan, and Mark Lundstrom. "Thermal transport at the nanoscale: A Fourier's law vs. phonon Boltzmann equation study." *Journal of Applied Physics* 121, no. 4 (2017).

18. Han Wang, Linfeng Zhang, Jiequn Han, and Weinan E. "DeePMD-kit: A deep learning package for many-body potential energy representation and molecular dynamics." *Computer Physics Communications* 228 (2018): 178-184.

19. Ikeshoji, Tamio, and Bjørn Hafskjold. "Non-equilibrium molecular dynamics calculation of heat conduction in liquid and through liquid-gas interface." *Molecular Physics* 81, no. 2 (1994): 251-261.

20. Thompson, Aidan P., H. Metin Aktulga, Richard Berger, Dan S. Bolintineanu, W. Michael Brown, Paul S. Crozier, Pieter J. In't Veld et al. "LAMMPS-a flexible simulation tool for particle-based materials modeling at the atomic, meso, and continuum scales." *Computer physics communications* 271 (2022): 108171.

21. McGaughey, Alan JH, and Jason M. Larkin. "Predicting phonon properties from equilibrium molecular dynamics simulations." *Annual review of heat transfer* 17 (2014).

22. Volz, Sebastian G., and Gang Chen. "Molecular-dynamics simulation of thermal conductivity of silicon crystals." *Physical Review B* 61, no. 4 (2000): 2651.

23. Cui, Haoran, Theodore Maranets, Tengfei Ma, and Yan Wang. "Spectral analysis of coherent and incoherent phonon transport in silicon nanomeshes." *Physical Review B* 110, no. 7 (2024): 075301.

24. Thomas, John A., Joseph E. Turney, Ryan M. Iutzi, Cristina H. Amon, and Alan JH McGaughey. "Predicting phonon dispersion relations and lifetimes from the spectral energy density." *Physical Review B* 81, no. 8 (2010): 081411.

25. Nosé, Shuichi. "A unified formulation of the constant temperature molecular dynamics methods." *The Journal of chemical physics* 81, no. 1 (1984): 511-519.

26. Hoover, William G. "Canonical dynamics: Equilibrium phase-space distributions." *Physical review A* 31, no. 3 (1985): 1695.

27. Kittel, Charles, and Paul McEuen. *Introduction to solid state physics*. John Wiley & Sons, 2018.

28. Born, Max, and Emil Wolf. *Principles of optics: electromagnetic theory of propagation, interference and diffraction of light*. Elsevier, 2013.

29. Luckyanova, Maria N., Jivtesh Garg, Keivan Esfarjani, Adam Jndl, Mayank T. Bulsara, Aaron J. Schmidt, Austin J. Minnich et al. "Coherent phonon heat conduction in superlattices." *Science* 338, no. 6109 (2012): 936-939.

30. Zeng, Lingping, Kimberlee C. Collins, Yongjie Hu, Maria N. Luckyanova, Alexei A. Maznev, Samuel Huberman, Vazrik Chiloyan et al. "Measuring phonon mean free path distributions by probing quasiballistic phonon transport in grating nanostructures." *Scientific reports* 5, no. 1 (2015): 17131.

31. Anufriev, Roman, Sergei Gluchko, Sebastian Volz, and Masahiro Nomura. "Quasi-ballistic heat conduction due to Lévy phonon flights in silicon nanowires." *ACS nano* 12, no. 12 (2018): 11928-11935.

32. Lee, Jaeho, Jongwoo Lim, and Peidong Yang. "Ballistic phonon transport in holey silicon." *Nano letters* 15, no. 5 (2015): 3273-3279.

33. Vakulov, Daniel, Subash Gireesan, Milo Y. Swinkels, Ruben Chavez, Tom Vogelaar, Pol Torres, Alessio Campo et al. "Ballistic phonons in ultrathin nanowires." *Nano letters* 20, no. 4 (2020): 2703-2709.

34. Cui, Haoran, Iyyappa Rajan Panneerselvam, Pranay Chakraborty, Qiong Nian, Yiliang Liao, and Yan Wang. "Significantly enhanced interfacial thermal transport between single-layer graphene and water through basal-plane oxidation." *Carbon* 234 (2025): 119910.